UMP-96/363

Tetragonal to Orthorhombic Transformation in Mg-PSZ

Z.W. Liu [a], A.E.C. Spargo [a], R.H.J.Hannink [b], J. Drennan [b,1]

[a] *School of Physics, The University of Melbourne, Victoria 3052, Australia*

[b] *Division of Materials Science, CSIRO, Clayton, Victoria 3168, Australia*

Abstract

The phase transformation from tetragonal to orthorhombic in MgO-partially-stabilized zirconia has been investigated by using high resolution transmission electron microscopy (HRTEM). Evidences are given to show that orthorhombic ZrO_2 frequently observed in transmission electron microscopy (TEM) thin foil studies was induced by dimpling and polishing during the specimen preparation. It was also found that the orthorhombic to monoclinic transformation was less sensitive to stress than the tetragonal to monoclinic transformation.

1. Introduction

Partially stabilized zirconia (PSZ) ceramics are generally produced by the addition of high temperature soluble oxide stabilizers such as MgO and CaO to zirconia. These zirconia-toughened ceramics usually comprise metastable precipitateds of tetragonal (t) zirconia and (in minor amounts) the monoclinic (m) polymorph of zirconia, in a matrix of cubic (c) stabilized zirconia. The martensitic transformation from tetragonal to monoclinic, which is accompanied by a volume increase of about 4%, makes an

[1] Present address: Center for Microscopy and Microanalysis, University of Queensland, St. Lucia, Qld 4072, Australia

important contribution to the toughening [1]. One of the toughest ceramics can be obtained by subjecting the sintered and control-cooled Mg-PSZ material to a final sub-eutectoid aging treatment at 1100°C. It has been confirmed [2] that significant quantity of δ-phase and a small quantity of orthorhombic (o) phase exist in Mg-PSZ samples which had been aged at sub-eutectoid temperature. The δ-phase, with the composition $Mg_2Zr_5O_{12}$ [3], has an cubic-related structure with ordered anion vacancies, and we will discuss it elsewhere.

The occurrence of orthorhombic phase in zirconia-toughened ceramics was first reported by Schoenlein and Heuer [4] in surface regions of "optimally-aged" Mg-PSZ. Heuer and co-workers also observed tetragonal to orthorhombic transformation either on fracture surfaces [5] or in thermally-shocked Mg-PSZ materials [6]. Orthorhombic ZrO_2 was also found in Ca-PSZ [7], and in Y_2O_3-ZrO_2 alloys [8].

The first evidence that o-phase occurred in substantial quantities was provided by Marshall *et al* [9] from X-ray diffraction examination of Mg-PSZ samples which had been cooled below about 170K. Marshall *et al* concluded that the tetragonal to orthorhombic transformation occurred throughout the bulk with most of the t-phase transformed to o-phase. By using neutron power diffraction analyses, Howard *et al* reported [10] that, upon cooling, an o-phase was produced in considerable quantities at the expense of the t-phase, and at 20K the sample contained about 38% by weight o-phase. The o-phase content increased to 45%, when the sample was warmed just about room temperature (307K). Although the orthorhombic to tetragonal reversion transformation occurred at 500K, small amount of the o-phase retained at 664K.

Marshall *et al* reported [9] that the formation of o-ZrO_2 in Mg-PSZ will lead to dramatic changes in mechanical properties of this high-toughness material. Its fracture toughness was reduced, and R-curve behavior was lost.

In this paper we report that most of the content of the o-phase in TEM thin foils was produced by dimpling and polishing during the specimen preparation.

2. Experimental Procedure

Mg-PSZ containing 9.4mol% MgO was prepared from mixed powders of the component oxides. The powder was sintered and solution-treated at 1700°C, cooled at 275°C/h to 1000°C, and then at 70°C/h to room temperature. The sample was reheated to 1100°C in air, aged for two hours, and then furnace-cooled.

Thin foils for electron microscopy were prepared from the sample. A disc of thickness about 1mm was cut and polished, and at this stage the thickness of the disc is about 200μm. Then the disc was cut into small discs with diameter about 3.5mm. Two discs were chosen. One was dimpled until the thickness of the center reaches about 30μm and then ion thinned. We named this one as specimen N_1. The other was ion thinned directly and we named it as specimen N_2.

A JEOL 4000EX high resolution transmission electron microscopy was used to examine the specimens at 400kV.

3. Experimental Results

3.1. Results from specimen N_1

Figure 1(a) is $\approx [00\bar{1}]_c$ zone axis selected area electron (SAE) diffraction pattern in which the extra reflections (weak points) appeared without characters of monoclinic

diffraction. These reflections (indexed based on cubic reflections, Figure 1(b)) are forbidden for both cubic and tetragonal t-ZrO_2 in this orientation. The (110) reflection could only come from o-ZrO_2 in $[001]_o$ zone axis diffraction while the (100), (010), (210) and (120) reflections could come from $[100]_o$, $[010]_o$, and $[001]_o$ orientations together. Figure 1(c) is a dark-field TEM image obtained using the (100), (010), (110), (210) and (120) reflections. The objective aperture position for taking the dark-field image is shown in Figure 1(b). The dark-field image shows that the tetragonal precipitates had transformed to o-ZrO_2 and the morphology of orthorhombic particle is identical with that of its t-ZrO_2 parent. Figure 2 is a high resolution micrograph showing images of two adjacent orthorhombic particles. These images had once been mistaken for m-ZrO_2 in the previous publications [11,12]. Figure 3 is a high resolution image showing part of a partially transformed orthorhombic particle with the m-ZrO_2 in $[010]_m$ orientation.

3.2. Results from specimen N_2

Figure 4(a) is also a $[001]_c$ selected area electron diffraction pattern. Although the (100), (010), (110), (210) and (120) reflections still appeared, the intensities of these reflections are much less than that of the cubic compared with Figure 1(a), and this indicates that the content of o-phase in specimen N_2 is less than that of specimen N_1. Figure 4(b) is a dark-field image obtained using these extra reflections. There are only a few tetragonal precipitates had transformed to o-ZrO_2 in the area of Figure 4(b) and all other tetragonal precipitates remained untransformed (compared with bright-field image, Figure 4(c)). Of the six particles, A,B,C,D,E and F showed in Figure 5(a), only particle A and B had transformed to o-phase (see dark-field image Figure 5(b)).

Figure 5(c) is a high resolution micrograph showing both orthorhombic particle (B) and tetragonal particle (C). Figure 5(d) and Figure 5(e) are the Fourier transforms of digitized selected image areas from particle B and C respectively. As expected, the (110) reflection is forbidden for t-phase but allowed for o-phase (arrowed, Figure(d)).

Figure 6(a) is another selected area electron diffraction pattern. The direction of the incident beam is defined parallel to $[0\bar{1}0]_c$ (in convention to index m-ZrO_2 reflections). Figure 6(c) and Figure 6(d) are dark-field images of adjacent areas. Figure 6(e) is the bright-field image of Figure 6(d). No tetragonal precipitate transformed to o-ZrO_2 in the area of Figure 6(c), while in the area of Figure 6(d) two laths (marked A and B) were observed. By re-examination the diffraction pattern (Figure 6(a)), we know that reflections from m-ZrO_2 in $[0\bar{1}0]_m$ orientation also appeared (indexed in Figure 6(b)). From Figure 6(e) we can see that the lath adjacent to lath A also transformed. Figure 6(f) is a high resolution image of the tetragonal precipitate containing lath A which confirmed that lath A had transformed to m-phase while the transformation was just initiated in adjacent lath (marked C). If the transformation proceeds further, lath C would transform to m-phase completely and the two m-ZrO_2 variants would be twin related. Why did the two m-ZrO_2 variants (A and B) showed light contrast here is because that the objective aperture used for taking dark-field image included the $(10\bar{2})_m$ reflection (Figure 6(e)) which came from $[0\bar{1}0]_m$ orientation diffraction. Other reflections included in the objective aperture may come from orthorhombic particles elsewhere. Even they may come from m-phase in $[100]_m$ or $[001]_m$ orientations, but these two orientations were rarely encountered for m-ZrO_2 in TEM observation.

4. Discussion

4.1. The structure of o-ZrO_2

Three different structures for *o*-ZrO_2 have been reported. The first crystal structure determination was attempted by Kudoh *etal* [13] using a diamond anvil pressure cell and in situ single crystal XRD. The results showed that the space group of *o*-ZrO_2 is *Pbcm*. Neutron diffraction studies [14,15] of the *o*-phase in cooled Mg-PSZ have shown that the low temperature structure has a space group $Pbc2_1$. Neutron diffraction work [16] on powders quenched from 600^{0}C and 6GPa showed that this high temperature and pressure *o*-phase has a structure with twice the *a* unit-cell parameter of others and space group *Pbca*. In thin foil TEM studies both structures with space group *Pbcm* [17] and *Pbca* [18] had been reported. The parameters of the three structures are list in Table 1.

It is obvious that the space group of the *o*-ZrO_2 found in our experiments is not *Pbca*, because the (110) reflection is forbidden for *o*-phase with space group *Pbca*. Image simulation showed that space group *Pbcm* is the best to fit calculated images with experiment results. Figure 7 is one of the calculated images which was frequently observed in HRTEM. The unit cell of the high pressure phase, with space group *Pbcm* determined by Kudoh *et al*, contains four molecules of ZrO_2. Four Zr atoms occupy the 4d site and four O atoms out of eight O atoms (denoted as O2) occupy 4c site and the remaining four O atoms (denoted as O1) occupy eight of the positions of the 8e site with equal probability.

4.2. The t to o transformation

The as-fired (not subjected to a sub-eutectoid aging treatment) Mg-PSZ sample contains no o-phase, but o-ZrO_2 was frequently observed in TEM thin foils, so it had once been suggested [7,17] that the formation of the o-phase from metastable tetragonal particles in TEM thin foils was an artifact. Muddle and Hannink [19] once showed that ion beam thinning can induce the tetragonal to orthorhombic transformation, and R. Suyama *et al* [20] found that grinding also can produce o-ZrO_2.

In our experiments we believe that most of the o-phase was induced by dimpling and polishing. The experiment results above show that most of the tetragonal precipitates had transformed to o-ZrO_2 in specimen N_1, while in specimen N_2 most tetragonal precipitates remained untransformed. Although the bulk sample contains 54.2% t-phase and only 2% o-phase [2], indeed we never detected t-ZrO_2 and frequently observed o-ZrO_2 in specimen N_1. Ion beam thinning moved off about 30μm of dimpled-surface of specimen N_1 and 200μm polished-surface of specimen N_2. No tetragonal precipitate was observed in the center observation area of specimen N_1, and this indicates that the transformation zone depth must be more than 30μm. Whereas in specimen N_2, t-ZrO_2 was abundant, while o-ZrO_2 was rarely encountered, therefore most of the transformation zone had been removed by ion beam thinning.

Polishing and dimpling transformed most of the tetragonal precipitates to o-phase other than m-phase. This may indicate that the tetragonal to orthorhombic transformation can be more easily induced than the tetragonal to monoclinic transformation. But we found that the o-ZrO_2 was not readily transformable by stress and this is consistent with what Marshall *et al* [9] noticed in cooled Mg-PSZ samples. Figure 8 is

a dark-field image showing a crack tip area found in specimen N_1. No orthorhombic particle transformed to m-ZrO_2 near the crack tip. Whereas, if the tetragonal precipitates had not been transformed to o-phase, cracking would lead to the transformation of tetragonal precipitates to m-phase. However, the orthorhombic to monoclinic transformation may be induced at high stresses, because m-ZrO_2 transformed from o-ZrO_2 can be observed like that shown in Figure 3.

5. Conclusions

(1) Polishing and dimpling are the two most important factors responsible for the tetragonal to orthorhombic transformation observed in TEM thin foil studies.

(2) The space group of orthorhombic ZrO_2 is *Pbcm* with its b axis parallel to the short dimension of the particle.

(3) The tetragonal to orthorhombic transformation can be more easily induced than the tetragonal to monoclinic transformation, while the o-ZrO_2 was not readily transformable by tensile stress.

Acknowledgements

The authors wish to thank Tom Bonin and David Dryden for assistance in specimen preparation.

REFERENCES

[1]. R. GARVIE, R. H. HANNINK, and R. T. PASCOE, *Nature*, **258**(1975)703-704.

[2]. R. H. J. HANNINK, C. J. HOWARD, E. H. KISI, and M. V. SWAIN, *J. Am. Ceram. Soc.*, **77**[2](1994)571-79.

[3]. H. J. ROSSELL and R. H. HANNINK, p.139, in Advances in Ceramics, Vol. 12, *Science and Technology of Zirconia II*

[4]. L. H. SCHOENLEIN and A. H. HEUER, *Fracture Mechanics of Ceramics*, Vol. 6, edited by R. C. Bradt, A. G. Evans, D. P. H. Hasselman, and F. F. Lange, Plenum, New York, (1982)309-323.

[5]. L. LENZ and A. H. HEUER, *J. Amer. Ceram. Soc.*, **65**(11)(1982)C192-194.

[6]. A. H. HEUER and L. H. SCHOENLEIN, *J. Mater. Sci.*, **20**(1985)3421-27.

[7]. R. M. DICKERSON, M. SWAIN and A. H. HEUER, *J. Amer. Ceram. Soc.*, **70**(4)(1987)214.

[8]. A. H. HEUER, R. CHAIM and V. LANTERI in proceedings of "ZrO_2 '86", in *Advances in Ceramics*, Vol. 24, edited by S. Somiya, N. Yamamoto and H. Yanagida, American Ceramic Society, Columbus, Ohio, 1988.

[9]. D. B. MARSHALL, M. R. JAMES, and J. R. PORTER, *J. Amer. Ceram. Soc.*, **72**(1989)218-27.

[10]. C. J. HOWARD, E. H. KISI, R. B. ROBERTS, and R. J. HILL, *J. Amer. Ceram. Soc.*, **73**(1990)2828-33.

[11]. A. H. HEUER, V. LANTERI and R. CHAIM, *Ultramicroscopy*, **22**(1987)27-34.

[12]. A. H. HEUER, *J. Am. Ceram. Soc.*, **70**(10)(1987)689-98.

[13]. Y. KUDOH, H. TAKEDA, and H. ARASHI, *Phys. Chem. Miner.*, **13**(1987)233-37.

[14]. E. H. KISI, C. J. HOWARD, and R. J. HILL, *J. Am. Ceram. Soc.*, **72**[9](1989)1757-60.

[15]. C. J. HOWARD, E. H. KISI, and O. OHTAKA, *J. Am. Ceram. Soc.*, **74**[9](1991)2321-23.

[16]. O. OHTAKA, T. YAMANOKA, S. KUME, N. HARA, H. ASANO, and F. IZUMI, *Proc. Jpn. Acad. Ser. B*, **66**(1990)193-96.

[17]. A. H. HEUER, V. LANTERI, S. C. FARMER, R. CHAIM, R. -R. LEE, B. W. KIBBLE, and R. M. DICKERSON, *J. Mater. Sci.*, **24**(1989)124-32.

[18]. A. H. HEUER, L. H. SCHOENLEIN, and S. FARMER, pp. 257-66, in *Science of Ceramics*, Vol. 12, edited by P. Vincenzini, Ceramurgica, Faenza, Italy, 1984.

[19]. B. C. MUDDLE and R. H. J. HANNINK, pp. 89-102 in Science and Technology of Zircinia III. Edited by S. Somiya, N. Yamamoto, and H. Yanagida, American Ceramic Society, Westerville, OH, 1988.

[20]. R. SUYAMA, T. ASHIDA, and S. KUME, *J. Am. Ceram. Soc.*, **68**[12](1985)C-314-C-315.

Table 1. Crystal Structure Models for o-ZrO_2

Atom		Kudoh *et al*	Kisi *et al*	Ohtaka *et al*
		*Pbcm**	$Pbc2_1$	*Pbca*
Zr	x	0.2683(8)	0.267(1)	0.2686(2)
	y	0.0334(2)	0.030(1)	0.0332(3)
	z	1/4	0.250(1)	0.2558(6)
O1	x	0.0822(79)	0.068(1)	0.0822(6)
	y	0.3750(21)	0.361(1)	0.3713(6)
	z	0.1292(22)	0.106(1)	0.1310(5)
O2	x	0.5436(54)	0.537(1)	0.5442(4)
	y	1/4	0.229(1)	0.2447(8)
	z	0	0	0.0052(6)

*a = 0.5005nm, b = 0.5235nm, c = 0.5051nm

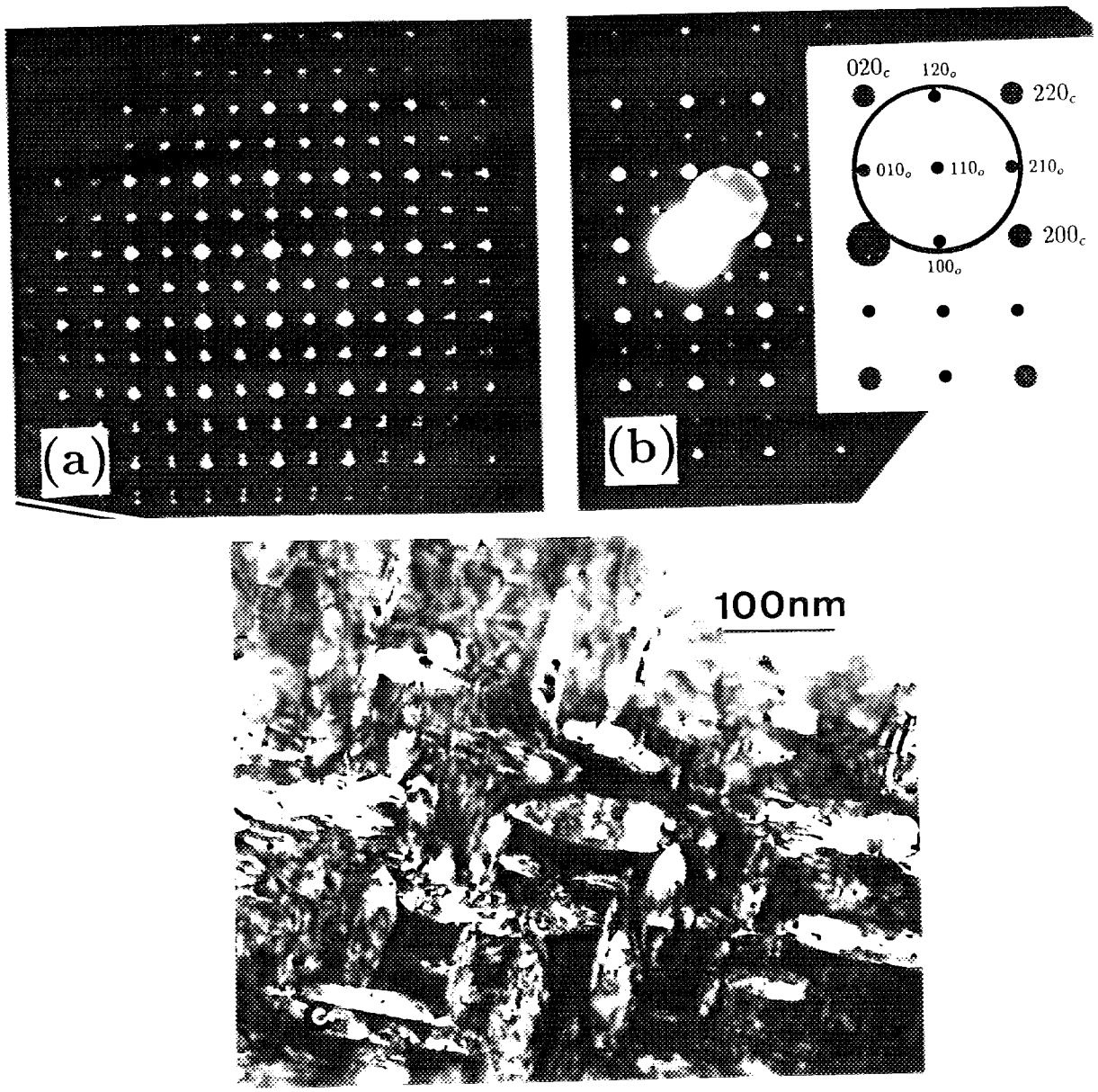

Figure 1: (a) SAE diffraction pattern with beam direction in $[001]_c$. (b) Objective aperture position ing dark-field image. (c) Dark-field image showing orthorhombic particles.

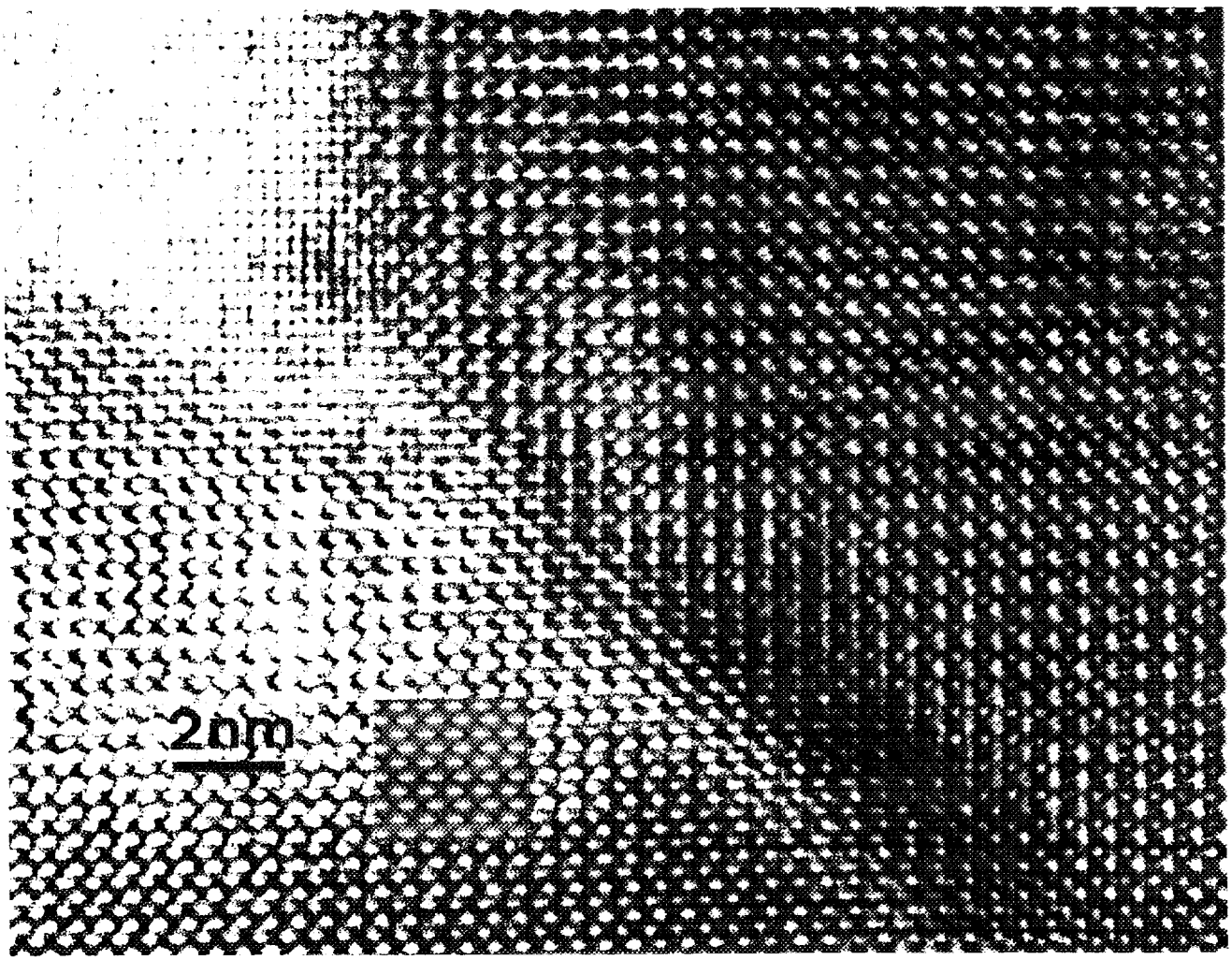

Figure 2: High resolution micrograph showing images of two adjacent orthorhombic particles in $[001]_o$ orientation (inset is a calculated image).

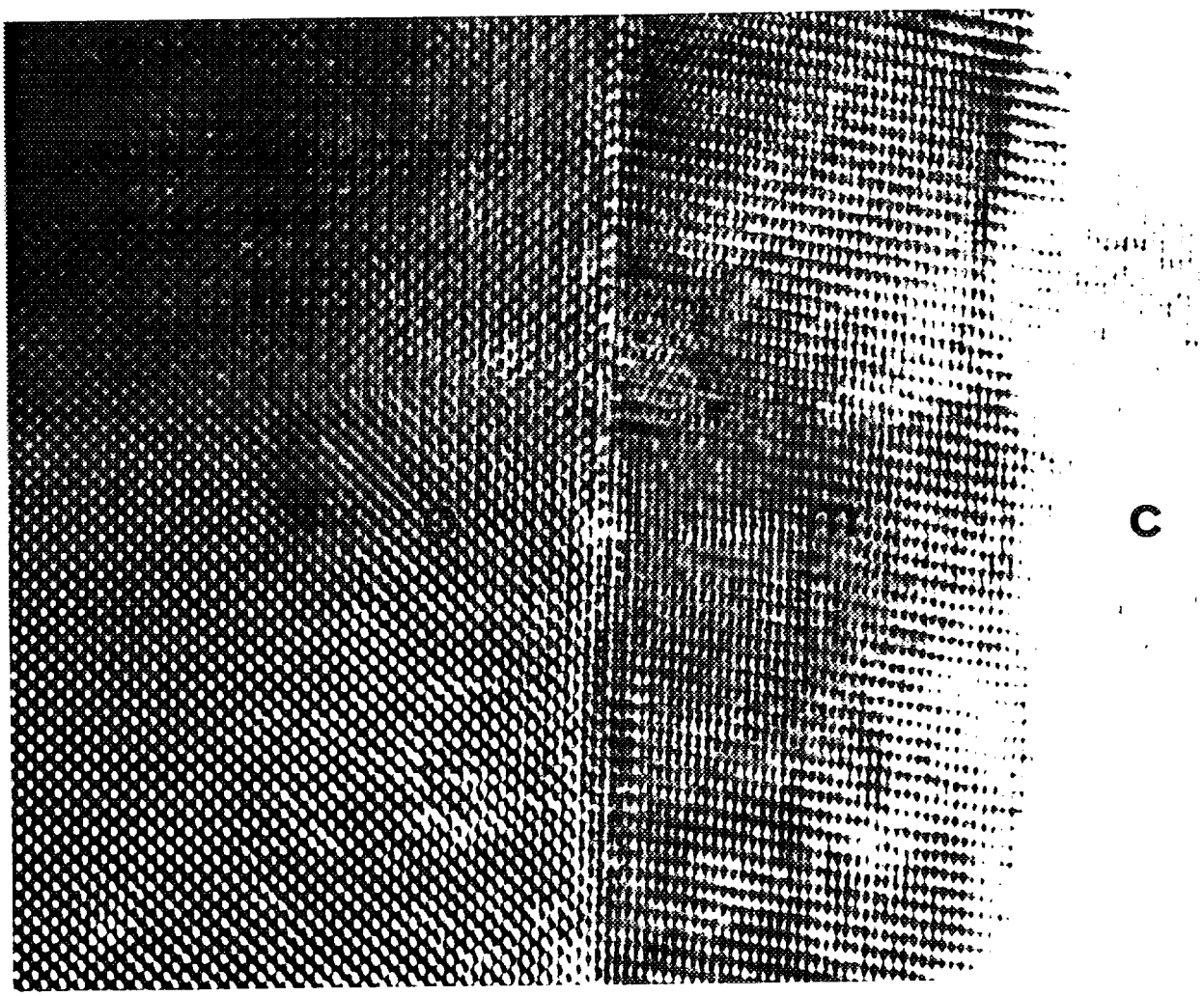

Figure 3: High resolution image showing part of a partially transformed orthorhombic particle.

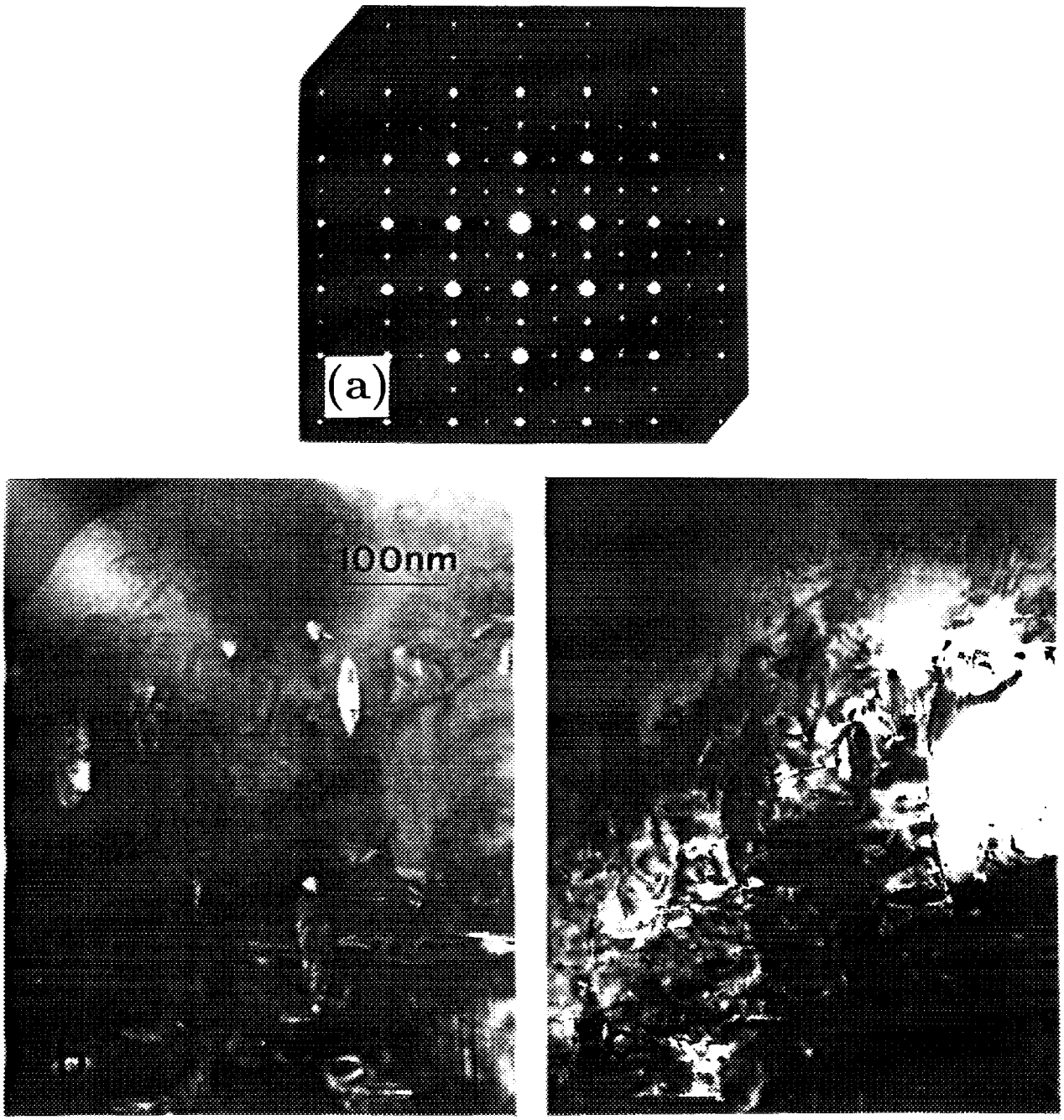

Figure 4: (a) $[001]_c$ SAE diffraction pattern. (b)Dark-field image showing orthorhombic particles. (c) Bright-field image showing both orthorhombic and tetragonal particles.

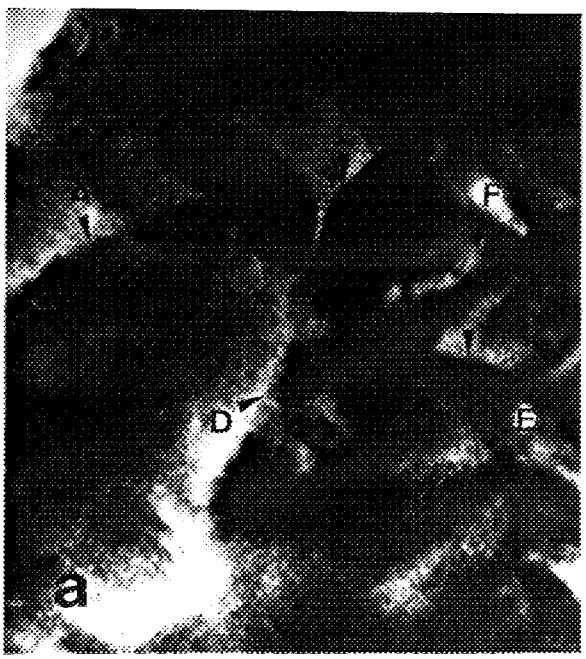
F
D
E
a

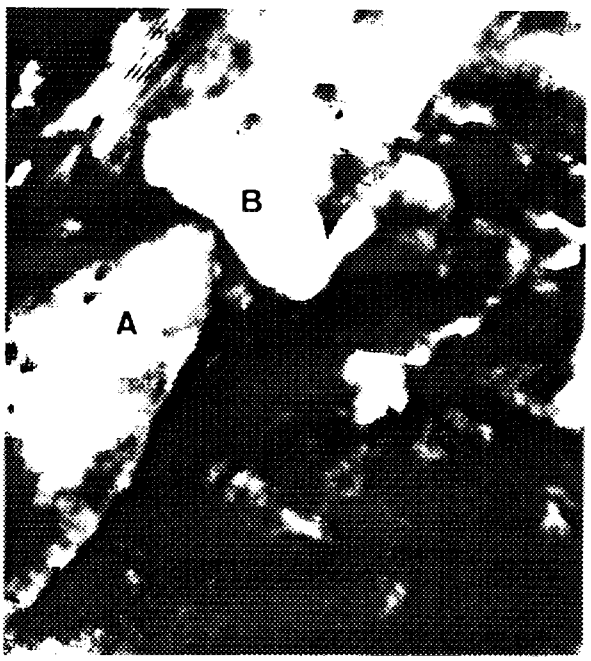
B
A

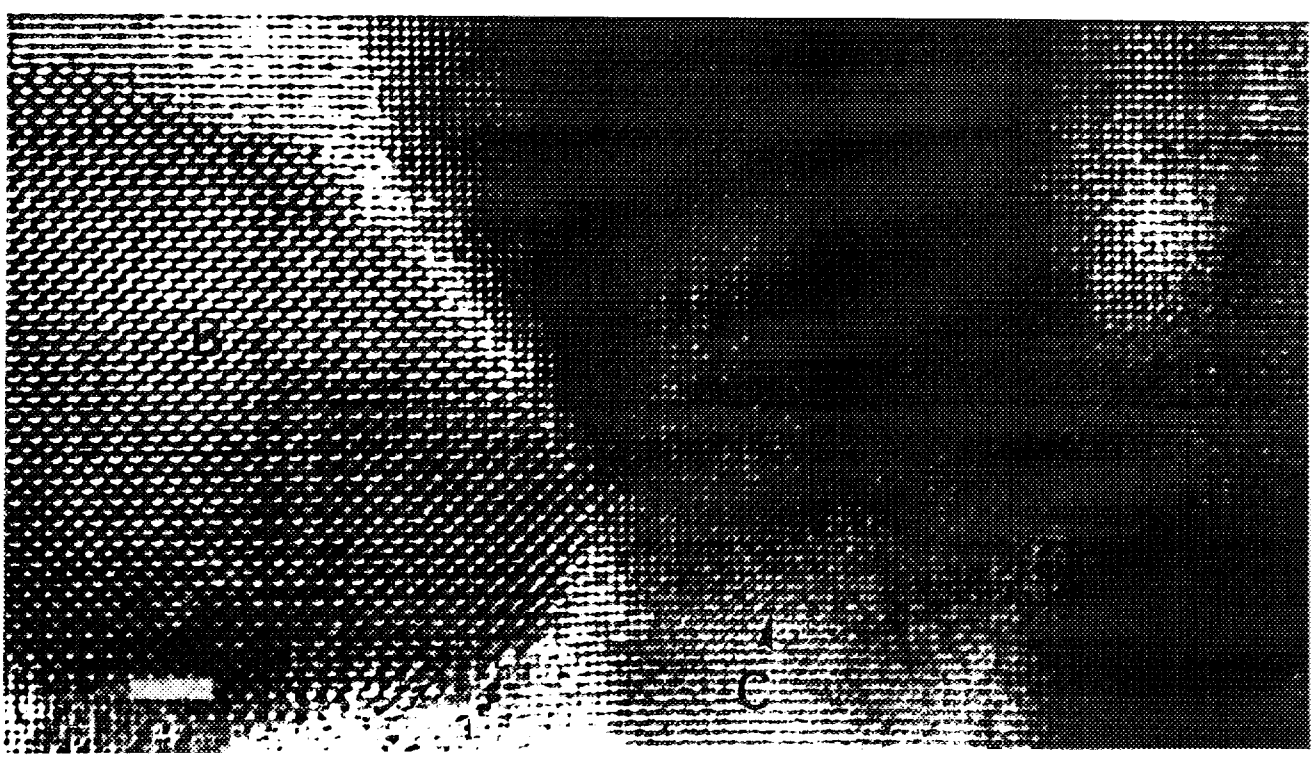
B
C

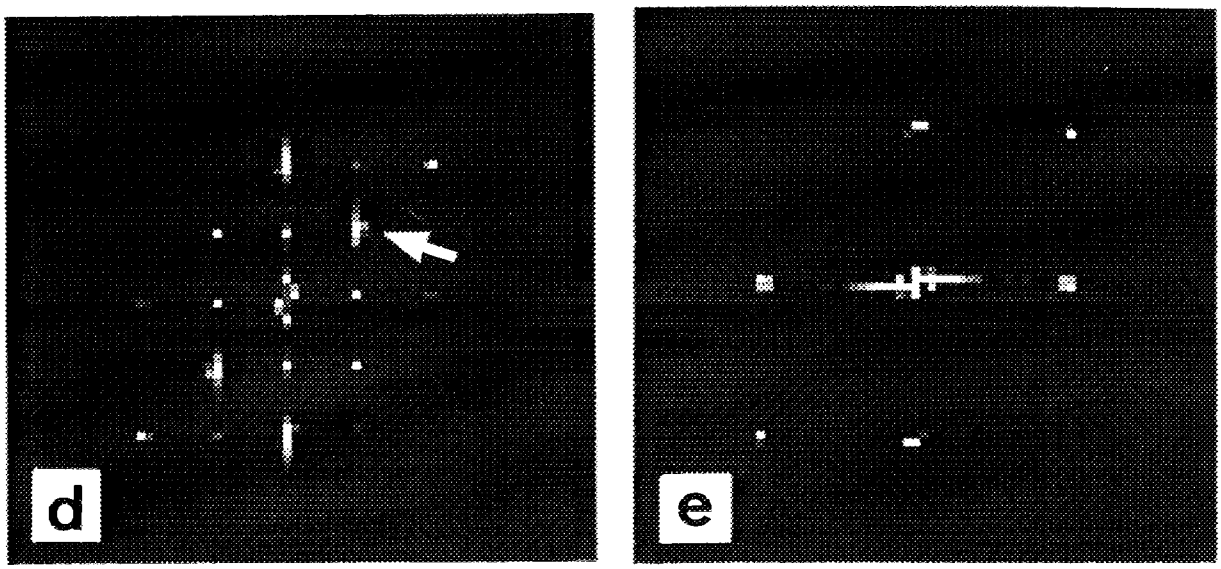

Figure 5: Bright-field (a) and dark-field (b) images showing both orthorhombic particles (A and B) and tetragonal particles (C, D, E and F). (c) High resolution micrograph showing images of particle B and C. (d) Fourier transform of digitized selected image area from orthorhombic particle (B). (e) Fourier transform of digitized selected image area from tetragonal particle (C).

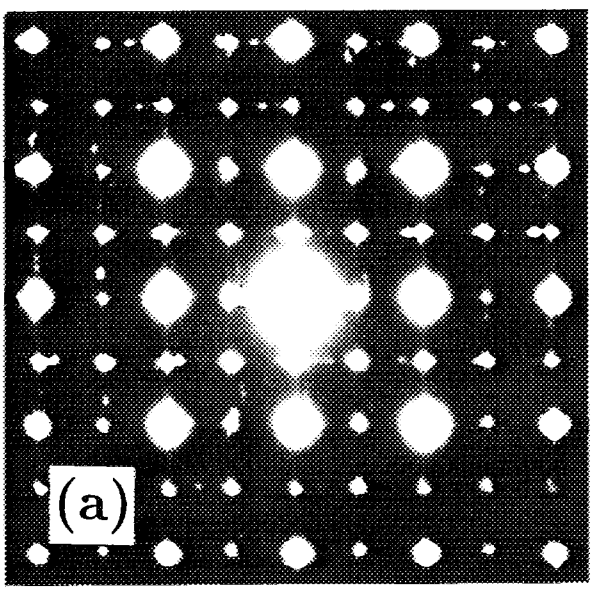

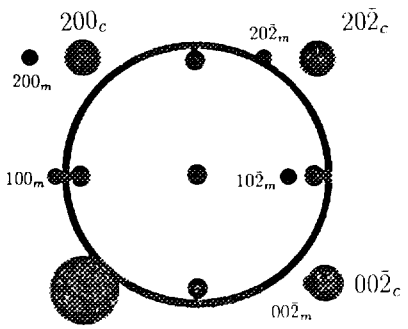

b

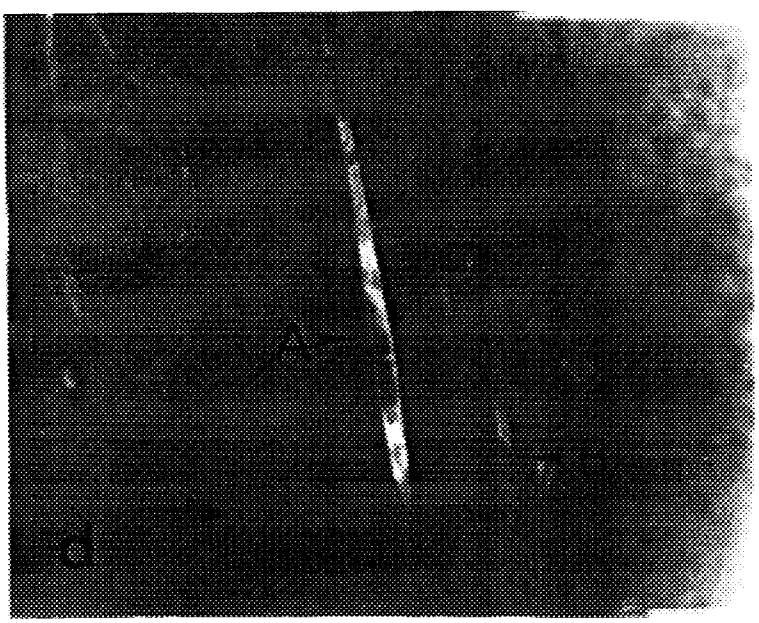

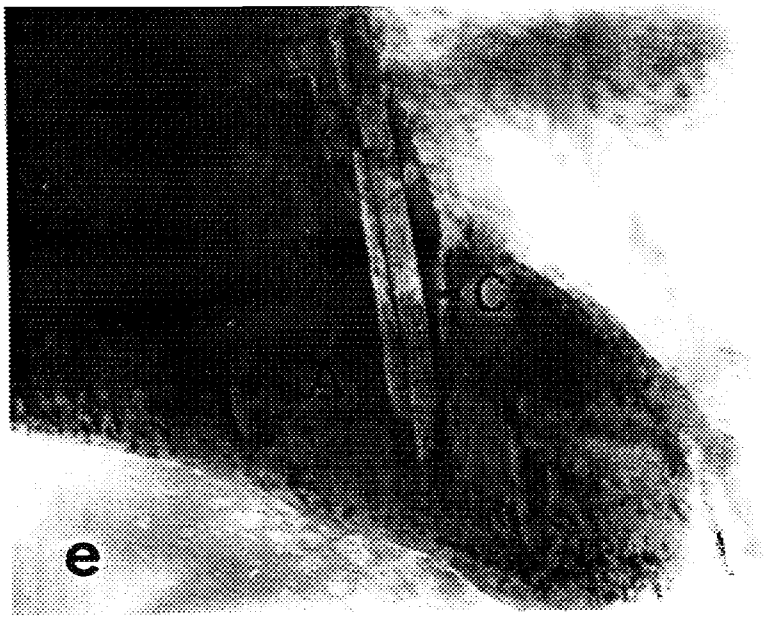

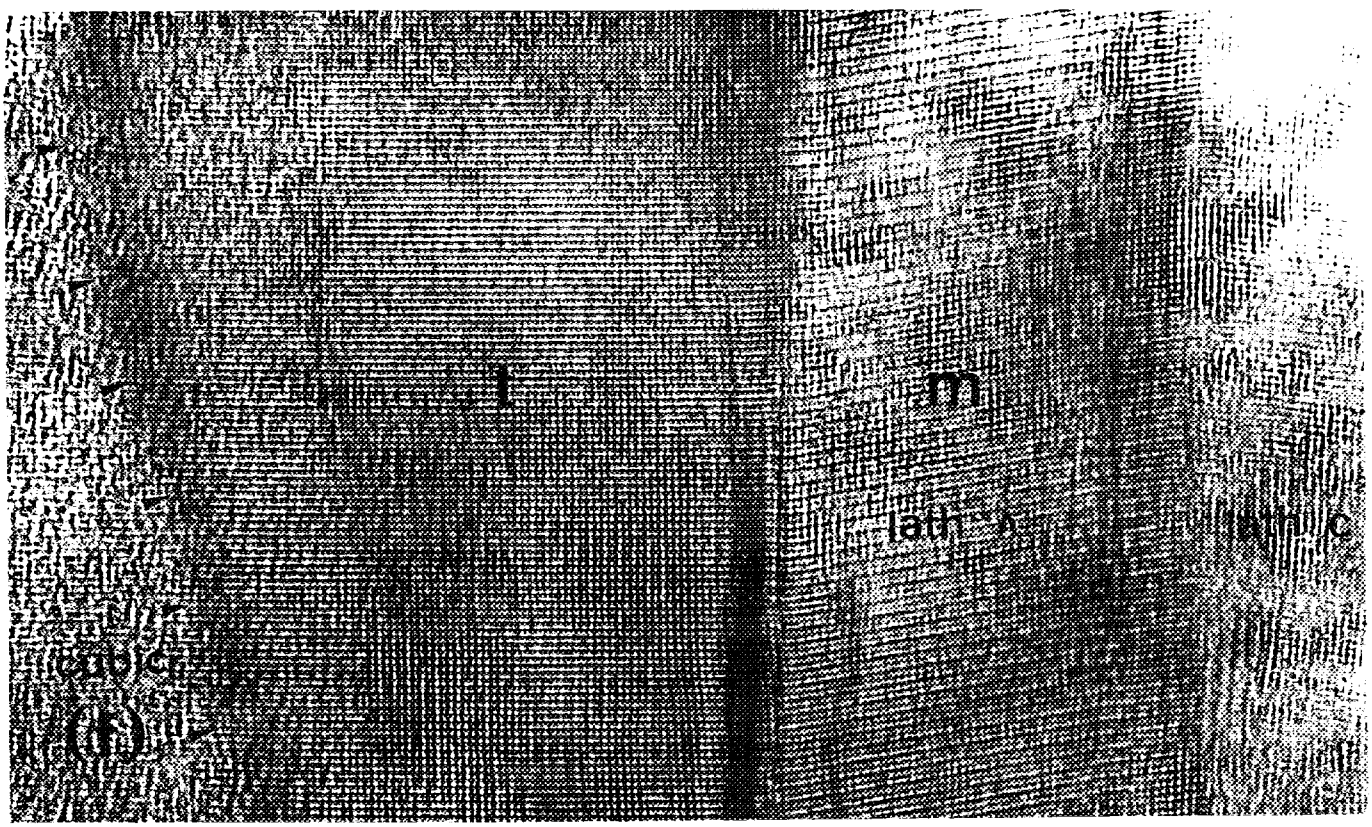

Figure 6: (a) $[0\bar{1}0]_c$ SAE diffraction pattern. (b) Objective aperture position for taking dark-field image. (c and d) Dark-field images of adjacent areas showing two (A and B) monoclinic variants. (e) Bright-field image of (d). (f) High resolution micrograph showing images of cubic, tetragonal and monoclinic in $[0\bar{1}0]_m$ orientation.

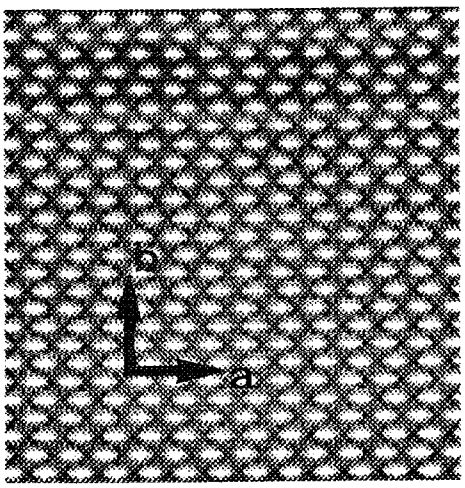

Figure 7: Calculated image of o-ZrO_2 in $[001]_o$ zone axis based on the structure reported by Kudoh *et al.*

Figure 8: Dark-field image showing orthorhombic particles near a crack tip.